Gamma, neutron, and muon-induced environmental background simulations for ^{100}Mo-based bolometric double-beta decay experiment at Jinping Underground Laboratory*

Wei Chen,[1] Long Ma,[1,†] Jin-Hui Chen,[1,‡] and Huan-Zhong Huang[1,2]

[1]*Key Laboratory of Nuclear Physics and Ion-beam Application (MOE), Institute of Modern Physics, Fudan University, Shanghai 200433, China*
[2]*University of California, Los Angeles, California 90095, USA*

The sensitivity of an experiment to detect the Majorana neutrino mass via neutrinoless double beta decay ($0\nu\beta\beta$) strongly depends on the rate of background events that can mimic this decay. One major source of this background is the radioactive emissions from the laboratory environment. In our study, we focused on assessing the background contributions from environmental gamma rays, neutrons, and underground muons to the Jinping bolometric demonstration experiment. This experiment uses an array of lithium molybdate crystal bolometers to probe the potential $0\nu\beta\beta$ decay of the ^{100}Mo isotope at the China Jinping Underground Laboratory. We also evaluated the shielding effectiveness of the experimental setup through an attenuation study. Our simulations indicate that the combined background from environmental gamma rays, neutrons, and muons in the relevant ^{100}Mo $0\nu\beta\beta$ Q-value region can be reduced to approximately 0.003 cts/kg/keV/yr.

Keywords: Neutrinoless double beta decay, Geant4, CUPID

I. INTRODUCTION

Unveiling the properties of neutrinos is fundamental, and searching for Neutrinoless double beta ($0\nu\beta\beta$) decay stands as a pivotal approach to this goal. Observing the $0\nu\beta\beta$ decay experimentally can directly substantiate the Majorana nature of neutrinos, implying that neutrinos are their own antiparticles. This would open new frontiers in physics, extending beyond the standard framework of particle physics [1].

Numerous experimental techniques have been employed to detect the rare $0\nu\beta\beta$ events. While direct evidence of $0\nu\beta\beta$ remains elusive, strict limits on the half-life of various double beta decay nuclides have been established [2–5]. Among the tools used, crystal bolometers, which operate at ultra-low temperatures, stand out. They are preferred for $0\nu\beta\beta$ searches due to their high energy resolution, efficient detection, and stable operation [6]. These cryogenic bolometers employ crystals embedded with double-beta decay isotopes to detect the $0\nu\beta\beta$ decay. The forthcoming CUPID experiment (CUORE with Particle Identification), integrating a high-performance heat-light dual readout to discern alpha particle backgrounds, is projected to enhance the sensitivity of $0\nu\beta\beta$ detection in the future [7–9].

A critical challenge in $0\nu\beta\beta$ detection is the potential interference from external radioactivity, as it can significantly hamper the experiment's potential. Efforts have thus been made to understand and mitigate sources of background interference. Previous research has identified multiple culprits for misleading counts in the $0\nu\beta\beta$ search energy region of interest (ROI), including cosmogenic activation, natural radioactive contamination from materials, and environmental radioactive emissions in the laboratory [10–14]. Given that cosmogenic activation at sea level notably influences the detectors, experiments are usually conducted in deep mines or under mountains; these locations, shielded by the earth's crust or mountain rock, offer protection from cosmic radiation [15, 16]. Besides residual cosmogenic background, environmental radioactive interference remains crucial for underground setups. Main sources include gamma rays from rocks, neutrons from surrounding materials, and events induced by underground muons [17, 18]. Passive shields are typically deployed to counter gamma and neutron backgrounds, while muon vetoes are used to effectively tag and exclude underground muon events and their induced activities.

Given that background levels are pivotal for experimental sensitivity, thorough studies on environmental background shielding and subsequent evaluations of any remaining background are crucial during the design phase of the detector system. In this paper, leveraging a Geant4-based Monte Carlo simulation, we delve into the background contributions—due to environmental gamma rays, neutrons, and cosmic muons—to the Jinping CUPID demonstration experiment. This experiment, featuring a 10 kg cryogenic crystal bolometer at the China Jinping Underground Laboratory (CJPL), aims to showcase the advanced technologies intended for the next-generation bolometric experiment targeting the $0\nu\beta\beta$ decay of ^{100}Mo. This paper is structured as follows: the simulation setup and methods are discussed in Sect. II. Findings related to particle attenuation and background are elaborated in Sect. III. Conclusions and discussions can be found in Sect. IV

II. SIMULATION SETUP

We utilized the Geant4 simulation toolkit (version 4.10.5) to model radiation shielding and assess background contributions [19]. Geant4 is renowned for offering an extensive array of particle-material interaction cross sections, allowing precise characterization of particle production and transport

* Supported in part by the State Key Research Development Program in China under Contract No.2022YFA1604702, No.2022YFA1604900, by the National Natural Science Foundation of China under contract No. 12025501, and by the Strategic Priority Research Program of Chinese Academy of Science with Grant No. XDB34030200.

† malong@fudan.edu.cn
‡ chenjinhui@fudan.edu.cn

properties [20–22]. For our study, we employed the "Shielding" physics list, which is tailored for simulations associated with deep underground rare event experiments. This physics list incorporates a series of interaction models, each detailing specific physical processes. For neutrons with energies up to 20 MeV, we leveraged high-precision models and cross-sections to depict processes such as elastic and inelastic scattering, capture, and fission. To study muon-induced backgrounds, we also applied the "QGSP_BERT" physics list as a supplementary check, given its suitability for cosmic ray-related processes. Event generation for gamma rays and neutrons was based on the in-situ spectral measurements taken in the CJPL experimental hall, as depicted in Fig. 1. We assumed isotropic radiation for both gamma and neutron sources. The initiation points for these environmental background sources were set in line with the hall's dimensions (14 m in height and 12 m in width). Moreover, the muon simulation factored in experimentally measured zenith and azimuthal angle distributions.

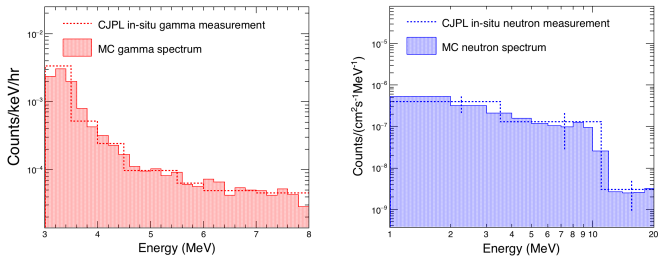

Fig. 1. (Color online) Energy spectra of CJPL environmental gamma (left) and neutron (right). The sampled Monte Carlo spectra (solid lines) are shown in comparison with the results obtained by the in-situ measurements (dashed lines) [23, 28].

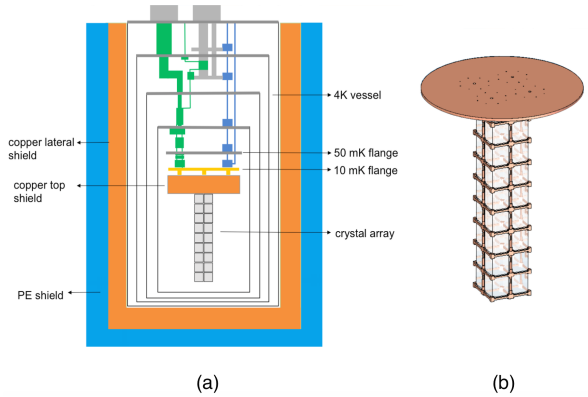

Fig. 2. Schematic view of the cryogenic system, shielding system (a), and crystal detector array (b) implemented in the Monte Carlo simulation.

Fig. 2 shows a schematic view of the experimental setup, including the detector crystal array, background shields surrounding the detector, and cooling system used to maintain low temperatures. The configurations of the detector and shielding systems are implemented in the simulation code. The CUPID-CJPL demonstrator comprised an array of thirty-six lithium molybdate (Li2MoO4) or LMO cryogenic bolometers, having a cumulative crystal mass of approximately 10 kg. The LMO crystals not only serve as the source for the $0\nu\beta\beta$ decay but also function as heat absorbers. This array is organized into nine layers, with each layer containing four bolometers. Each of these bolometers is cooled to an ultra-low temperature of about 10 mK using a dilution refrigerator. The individual bolometer module integrates a $4.5\times4.5\times4.5$ cm^3 LMO cubic crystal and is equipped with a heat-light dual-phase readout. For these modules, 280 g LMO crystals were specifically chosen. The cooling apparatus, or the cryostat, consists of three concentric vessels dedicated to thermal shielding. To complement these thermal barriers, radiation shields were strategically positioned both inside and surrounding the cryostat to counteract radiation emanating from the cryogenic system. Within this arrangement, a substantial copper shield (having a thickness of 12 cm and a diameter of 50 cm) was situated above the detector tower to mitigate external radioactive interference. To further fortify the system, passive shielding materials were employed. This includes a 12 cm thick layer of copper, designed to diminish environmental gamma rays, and a 20 cm thick layer of 5%-borated polyethylene (PE) tailored to intercept environmental neutrons. The salient features of this experimental setup are detailed in Table 1.

Table 1. Key elements of the experimental setup.

Element	Material	Mass (kg)	Surface (cm^2)
Crystal array	LMO	10.0	4374.0
Thermal shield	Cu-OFE	61.7	23850.9
Top Cu shield	Cu-OFE	209.7	4736.9
Lateral Cu shield	Cu-OF	2990.4	60880.0
Lateral PE shield	PE	1343.9	114300.0

III. RESULTS AND DISCUSSION

A. Attenuation study

Numerous experimental studies have established that materials with high atomic mass numbers, such as lead and copper, excel at attenuating gamma rays. Notably, copper typically possesses lower inherent radioactivity than lead. As a result, high-purity oxygen-free copper has emerged as a preferred material for crafting shielding systems in sensitive underground experiments related to rare events.

For the Jinping bolometric demonstration, the design of the background shielding system was informed by a Monte Carlo simulation. Utilizing the Geant4 toolkit, we simulated particle interactions with materials to quantitatively assess the attenuation capacities of the shielding against gamma rays and neutrons.

Fig. 3 shows the gamma-ray absorption fraction as a function of the gamma energy for different copper shielding thicknesses. The incident gamma energy was sampled based on

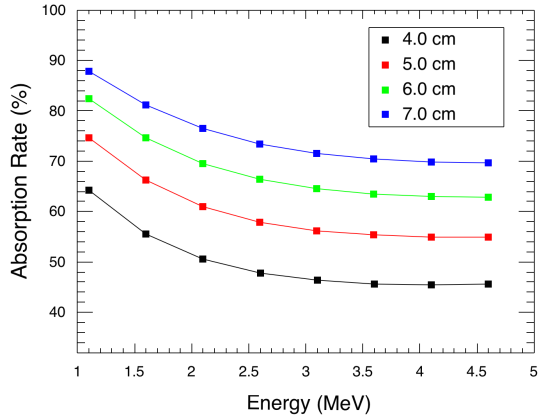

Fig. 3. (Color online) Simulated results of the gamma absorption for varying thicknesses of the copper brick.

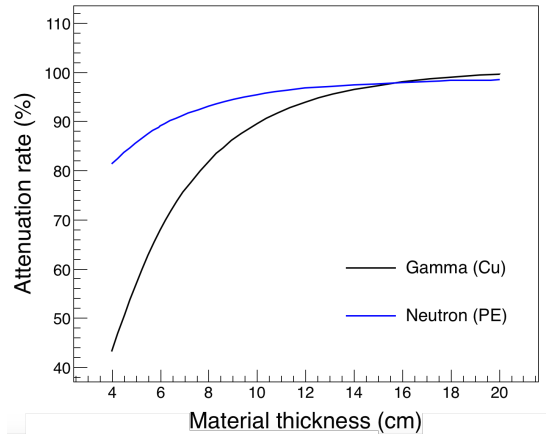

Fig. 4. (Color online) Simulated results of the attenuation coefficient as a function of copper shielding thickness for gamma and borated polyethylene thickness for neutron. The input energy spectra for gamma and neutron are shown in Fig. 1.

the experimentally measured CJPL in situ gamma spectra. 1. Our results indicate that the gamma absorption at different energies improves significantly by increasing the thickness of the material. In addition to high-energy environmental gamma rays, fast neutrons with energies above 1 MeV are serious background sources for rare underground event experiments. Borated polyethylene (BPE) is an effective material for fast neutron shielding [24, 25]. The results of the neutron-shielding performance are shown in Fig. 4 compared with the gamma results. The black and blue curves represent the gamma and neutron absorptions of copper and 5% BPE, respectively. It was observed that the neutron shielding was improved by increasing the thickness of BPE. A reduction in gamma and neutron fluxes by a factor of ∼10 can be realized by deploying a 12-cm thick copper shield and an 8-cm 5% BPE shield, respectively. Thus, for the CJPL bolometric experiment, with 12-cm thick copper and 20-cm thick 5%-borated polyethylene external shields, we expect a reduction exceeding 10-fold in the environmental gamma and neutron fluxes within the detector system.

B. Environmental gamma induced background

Different background sources have the potential to simulate a $0\nu\beta\beta$ signal within the decay-energy ROI of $0\nu\beta\beta$. A predominant source of such radiation is environmental gamma rays. For underground experiments, these gamma rays largely stem from the decay of radioactive nuclei and processes induced by high-energy neutrons. Moreover, the lab's infrastructure and its experimental apparatus can introduce additional gamma background. In our research, we delved into evaluating the contribution of environmental gamma background to a ^{100}Mo $0\nu\beta\beta$ detection using a bolometric method.

The gamma radioactivity of the CJPL environment has been extensively profiled in prior studies through in-situ gamma-ray measurements employing a high-purity germanium spectrometer [26–30]. The naturally occurring gamma spectrum spans up to 3 MeV; events exceeding this energy are typically the result of interactions between neutrons, muons, and rocks. Given that the isotope ^{100}Mo boasts a relatively high $Q_{\beta\beta}$ value (approximately 3034.40(17)keV), we designated the ROI to range from 3000–3060 keV. This decision factored in the energy resolution of the crystal bolometer when assessing the background. The approach to parameterizing the energy resolution is as follows:

$$\sigma(E) = \sqrt{0.49 + (0.058 \times \sqrt{E})^2}, \quad (1)$$

where E denotes the measured energy in keV based on the CUPID-Mo study [31].

The gamma spectrum measured using a high-purity germanium (HPGe) detector in CJPL Phase II was used as the input for our Geant4 simulation [26]. In this study, given that we focused on the ^{100}Mo $0\nu\beta\beta$ ROI, only high-energy gamma-rays (E_γ>3000 keV) were considered. The integral flux of the high-energy gamma rays was calculated as 2.51 ± 0.07 × 10^{-6} $cm^{-2}s^{-1}$ based on the experimentally measured results.

In bolometric experiments, the array structure of the detector system allows us to apply the anti-coincidence cut criterion. This helps in rejecting high-energy external background events that pass through several crystal modules. Fig. 5 illustrates the concept of "$multiplicity$". An event that deposits energy in a single crystal module is defined as having "$multiplicity = 1$". Conversely, if the energy is deposited across multiple crystal modules, it's classified as a "$multiplicity > 1$" event. By selecting the "$multiplicity = 1$" events, we can significantly filter out high-energy external gamma rays, as well as neutrons and muons, that traverse multiple crystals.

Fig. 6 presents the simulated results for the gamma-induced background. The results for different cutting criteria are shown for comparison. It is observed that by requiring "$multiplicity = 1$", the environmental gammas contribute

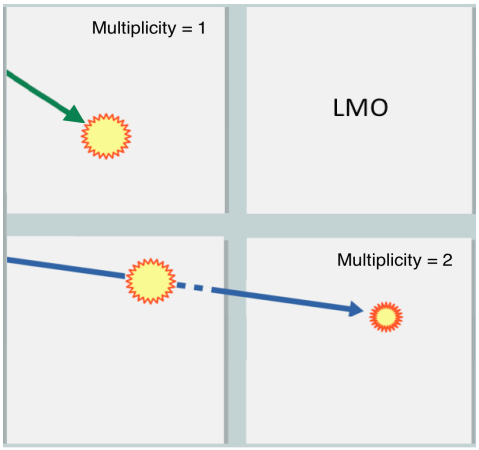

Fig. 5. (Color online) Definition of the multiplicity.

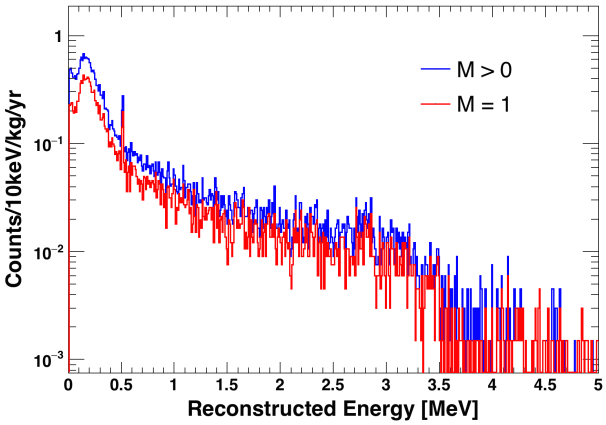

Fig. 6. (Color online)Simulated results of the gamma-induced background.

approximately 1.3 $\times$ 10^{-3} cts/keV/kg/yr background in the ^{100}Mo $0\nu\beta\beta$ ROI (3000-3060 keV). The uncertainty of the result is estimated by considering the statistical uncertainties of the flux measurements and selection of PhysicsList ("Shielding" vs "QGSP_BERT_HP"). The relative difference was found to be within 10%.

C. Environmental neutron induced background

High-energy neutrons present another significant background for $0\nu\beta\beta$ experiments. In deep underground laboratories, neutron fluxes below 10 MeV primarily arise from spontaneous fission (such as from U-238) and (α,n) reactions, which involve interactions between alphas from natural radioactive sources and light target nuclei within the rock. Beyond production by the inherent radioactivity of materials, neutrons can also be produced by cosmic-ray muons and their secondary particles through nuclear reactions [32, 33]. The energy of these muon-induced neutrons can reach up to several gigaelectronvolts.

Systematic measurements of the fluxes of low-energy thermal neutrons and high-energy fast neutrons have been performed in deep underground laboratories [23, 34–36]. In our simulation study, we evaluated the neutron-induced background based on the in situ fast neutron spectrum measured at the CJPL Hall-A [37]. Monte Carlo neutrons with kinetic energies exceeding 1 MeV were sampled based on the experimental flux spectrum results. The total flux was approximately (1.51 $\pm$ 0.03) $\times$ 10^{-7} $cm^{-2}s^{-1}$ for E_n>1 MeV without the polyethylene shielding. The results for the residual neutron-induced background with the copper and PE shielding setups are shown in Fig. 7. We observed that the environmental neutrons contribute approximately 1.6 $\times$ 10^{-3} cts/keV/kg/yr in the ^{100}Mo $0\nu\beta\beta$ ROI with "$multiplicity = 1$" cut applied. It should be noted that there are currently no published experimental data on CJPL environmental neutron flux exceeding 20 MeV. Thus, high-energy neutrons (E_n>20 MeV) were not considered in our simulations. Nevertheless, according to existing simulation studies performed for LNGS, the integral flux exceeding 10 MeV (mainly from muon-induced processes) is three orders of magnitude lower than that below 10 MeV (mainly from radioactivity-induced processes) [38, 41]. For the CJPL, owing to the larger depth, the flux of cosmic-muon-induced neutrons was even lower. The relative background contribution from E_n>20 MeV high energy neutron was expected to be low.

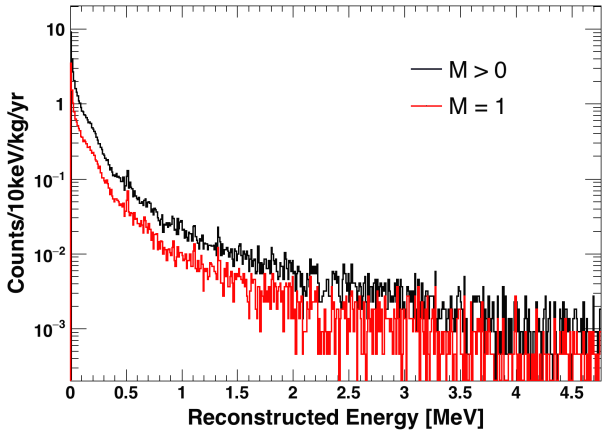

Fig. 7. (Color online) Simulated results of the neutron-induced background.

D. Underground cosmic muon induced background

Cosmogenic backgrounds play a pivotal role in rare-event search experiments [39]. At Earth's surface, cosmic rays predominantly consist of high-energy muons [40]. The significant rock overburden of CJPL (equivalent to 6700 m of water) dramatically reduces the cosmic muon flux underground—by about eight orders of magnitude compared to the flux at sea level. As a result, the cosmogenic background doesn't pose a significant threat to the Jinping bolometric experiments. Nevertheless, for the heightened sensitivity objectives of upcoming $0\nu\beta\beta$ experiments, a thorough evaluation of the residual

muon-induced background is imperative.

To estimate the muon-induced background level, it's essential to understand both the energy and angular distributions of underground muons in a given experimental cavern. The muon energy was derived using a parametric function [41]:

$$\frac{dN}{dE_\mu} = Ce^{-bh(\gamma_\mu - 1)}(E_\mu + \varepsilon_\mu(1 - e^{-bh}))^{-\gamma_\mu}, \quad (2)$$

where $b = 0.4/km.w.e$, $\gamma_\mu = 3.77$, and $E_\mu = 693\ GeV$ were used, as suggested.

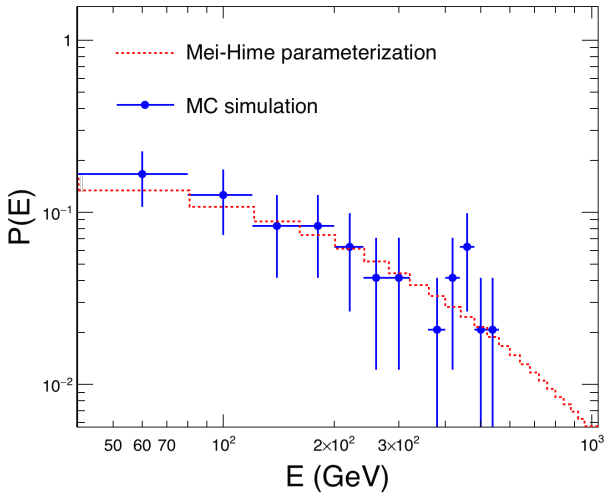

Fig. 8. (Color online) Energy spectrum of the CJPL muons. Results from the parametric function are shown in comparison with that from the Monte Carlo simulation.

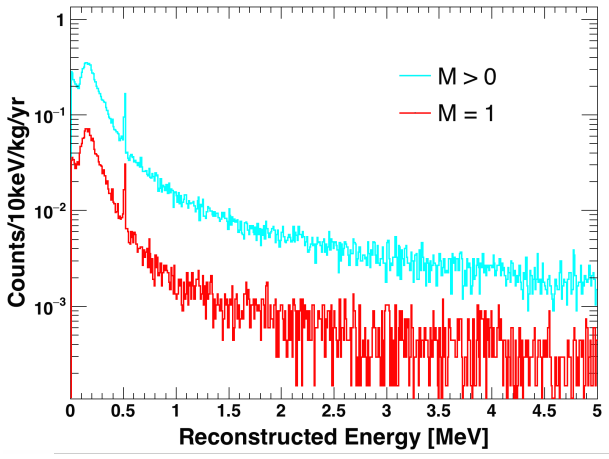

Fig. 9. (Color online)Simulated results of the muon-induced background contribution.

Fig. 8 shows the underground muon spectrum from a Geant4-based simulation study and compares it with the Mei-Hime parameterization results [42]. The parametric function accurately described the Geant4 simulation results. For the angular distribution, additional information regarding rock overburden is required to determine the flux in a specific direction. In this study, the zenith and azimuthal angle distributions of the underground muons were sampled according to JNE measurements [43]. The experimental distributions can be described using the parametric function discussed in Ref. [44]. The total underground muon flux used as the input for the simulation was $3.53 \times 10^{-10}\ cm^{-2}s^{-1}$ based on the measurement at CJPL Phase II.

The simulated results of the muon-induced background contributions are shown in Fig. 9. We observed that the background contribution of muon events, including muon-induced secondaries, corresponds to a low level of 2.2×10^{-5} cts/keV/kg/yr in the ^{100}Mo $0\nu\beta\beta$ ROI. It was also observed that the multiplicity anti-coincidence cut significantly suppressed the muon-induced background by an order of magnitude.

IV. CONCLUSION

We conducted a simulation study evaluating the background shielding for the Jinping ^{100}Mo-based bolometric demonstration experiment aimed at searching for neutrinoless double-beta decay. Having established the shielding arrangement through an attenuation study, we assessed the environmental gamma, neutron, and muon-induced backgrounds. Our findings indicate that within the ^{100}Mo $0\nu\beta\beta$ ROI, gamma rays and neutrons contribute to background levels of approximately 1.3×10^{-3} cts/keV/kg/yr and 1.6×10^{-3} cts/keV/kg/yr, respectively. The underground cosmic ray muon's contribution was minor, only reaching 2.2×10^{-5} cts/keV/kg/yr in the ROI when the anti-coincidence cut was applied. Additionally, given the bolometer's slow data acquisition rate, potential pile-up events, notably coincident low-energy gamma rays, could also add to the discernible experimental background. It's worth noting that our simulations were done for a demonstration experiment without supplementary passive background shielding. In CJPL Phase II, a meticulously designed combined shielding apparatus (comprising 20 cm of lead and 100 cm of PE) was implemented for radioactive background protection. We anticipate a significant reduction in the combined contributions from environmental gamma and neutron backgrounds to levels below 10^{-3} cts/keV/kg/y, aligning with our objectives for this demonstration experiment. For the $0\nu\beta\beta$ experiment, background plays a pivotal role, directly influencing experimental sensitivity. Therefore, curbing background contribution emerges as a critical facet of bolometric experimental studies and advancements. Regarding the environmental background, precise in-situ measurements of both neutron and gamma spectra, extending into high-energy regions, are paramount for designing shielding systems tailored to future high-sensitivity $0\nu\beta\beta$ research endeavors at CJPL

V. BIBLIOGRAPHY

[1] S.M. Bilenky, C. Giunti, Int. J. Mod. Phys. A 30, 1530001 (2015)
[2] Adams, D. Q. *et al.* (CUORE collaboration), Phys. Rev. Lett. 124, 122501 (2020)
[3] Albert, J. B. *et al.* (EXO collaboration), Phys. Rev. Lett. 120, 072701 (2018)
[4] Agostini, M. *et al.* (GERDA collaboration), Phys. Rev. Lett. 120, 132503 (2018)
[5] Gando, A. *et al.* (KamLAND-Zen collaboration), Phys. Rev. Lett. 117, 082503 (2016)
[6] M. Biassoni, O. Cremonesi, Progress in Particle and Nuclear Physics 114, 103803 (2020)
[7] Armstrong, W. R. *et al.* (The CUPID Interest Group), arXiv:1907.09376
[8] Armengaud, E. *et al.* (CUPID collaboration), Phys. Rev. Lett. 126, 181802 (2020)
[9] E. Armengaud *et al.*, Eur. Phys. J. C 80:674 (2020)
[10] A. Alessandrello *et al.*, Nuclear Instruments and Methods in Physics Research B 142, 163-172 (1998)
[11] A. Luqman *et al.*, Nuclear Instruments and Methods in Physics Research A 855, 140-147 (2017)
[12] F. Alessandria *et al.* (CUORE collaboration), Astroparticle Physics 45, 13-22 (2013)
[13] H.W. Bae, E.J. Jeon, Y.D. Kim, S.W. Lee, Astroparticle Physics 114, 60-67 (2020)
[14] C. Alduino, K. Alfonso *et al.* (CUORE collaboration), Eur. Phys. J. C 77:543 (2017)
[15] W. Chen, L. Ma, J. H. Chen, H. Z. Huang, Y. G. Ma, Eur. Phys. J. C 82:549 (2022)
[16] Patrick N. Peplowski *et al.*, Nuclear Instruments and Methods in Physics Research B 446, 43-57 (2019)
[17] F.Bellini, C.Bucci, S.Capelli, O.Cremonesi, L.Gironi, M.Martinez, M.Pavan, C.Tomei, M.Vignati, Astroparticle Physics 33, 169-174 (2010)
[18] Marijke Haffke, Laura Baudis, Tobias Bruch *et al.*, Nuclear Instruments and Methods in Physics Research A 643, 36-41 (2011)
[19] J. Allison *et al.*, Nucl. Instrum. Methods A, 835, 186 (2016)
[20] S. Agostinelli *et al.*, Nucl. Instrum Methods A 506, 250 (2003)
[21] Da-Jun Zhao, Song Feng, Pin-Jing Cheng *et al.*, Nuclear Science and Techniques 34(1):3(2023)
[22] Li-Heng Zhou, Shui-Yan Cao, Tao Sun *et al.*, Nuclear Science and Techniques 34(4):54(2023)
[23] Q. D. Hu, H. Ma, Z. Zeng *et al.* Nuclear Instruments and Methods in Physics Research A 859, 37-40 (2017)
[24] Y. Elmahroug, B. Tellili and C. Souga, International Journal of Physics and Research 3(1), 33-40 (2013)
[25] D Venkata Subramanian, Adish Haridas, D Sunil Kumar, A John Arul and P Puthiyavinayagam, Indian Journal of Pure and Applied Physics 56, 583-586 (2018)
[26] H. Ma, Z. She *et al.*, Astroparticle Physics 128, 102560 (2021)
[27] Z. Zeng, J. Su, H. Ma *et al.*, Journal of Radioanalytical and Nuclear Chemistry 301(2) (2014)
[28] Y. P. Shen, J. Su, W. P. Liu *et al.*, Science China Physics, Mechanics and Astronomy 60(10),102022 (2017)
[29] L. Li, Q. Yue, C. J. Tang *et al.*, Chinese Phys. C 35, 282 (2011)
[30] Ren-Ming-Jie Li, Shu-Kui Liu, Shin-Ted Lin *et al.*, Nuclear Science and Techniques 33(5):57(2022)
[31] Schmidt, B. *et al.*, J. Phys. Conf. Ser. 1468(1), 012129 (2020)
[32] B. Aharmim *et al.*, Phys. Rev. D 100, 112005 (2019)
[33] V. A. Kudryavtsev, N. J. C. Spooner, J. E. McMillan, arXiv:hep-ex/0303007v1 (2003)
[34] Z. M. Zeng *et al.*, Nucl. Instrum. Meth. A 804, 108-112 (2015)
[35] G. Bruno and W. Fulgione, Eur. Phys. J. C 79:747 (2019)
[36] Q. H. Wang, A. Abdukerim, W. Chen *et al.*, Science China: Physics, Mechanics and Astronomy 63(3):231011
[37] Q. Du, S.T. Lin, S.K. Liu *et al.* Nuclear Instruments and Methods in Physics Research A 889, 105-112 (2018)
[38] H. Wulandari *et al.*, Astroparticle Physics 22, 313 (2004)
[39] E. Andreotti, C. Arnaboldi *et al.*, Astroparticle Physics 34, 18-24 (2010)
[40] PThomas K. Gaisser, Cosmic Rays and Particle Physics (Cambridge University Press, New York, 1990), p. 71.
[41] D. M. Mei and A. Hime, Physical Review D 73, 053004 (2006)
[42] X. H. Hu, Simulation of cosmic ray background at CJPL, Master's Dissertation, Nankai University, 2013
[43] Z. Y. Guo, L. B. Peters, S. M. Chen *et al.* Chinese Physics C 45, 2 (2021)
[44] H. Arslan and M. Bektasoglu, Advances in High Energy Physics 2013, 391573